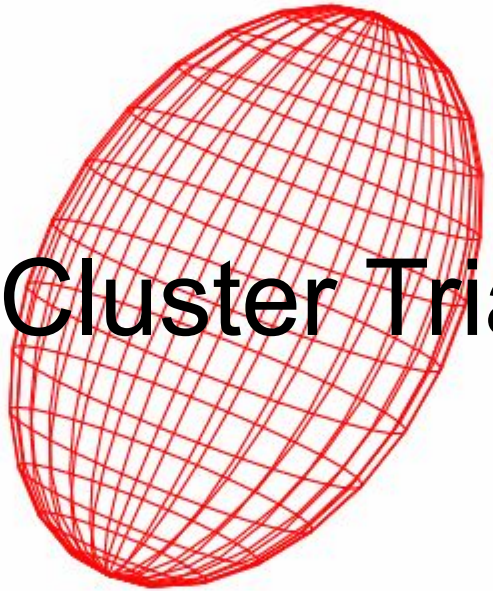
Galaxy Cluster Triaxiality



Radhakrishnan Srinivasan
Postdoctoral Fellow, Southern Methodist University

Cluster triaxiality project - Paper I

Applying the CLMM triaxiality module to real data and simulated data and preparing for Rubin

The paper has been accepted by ApJ

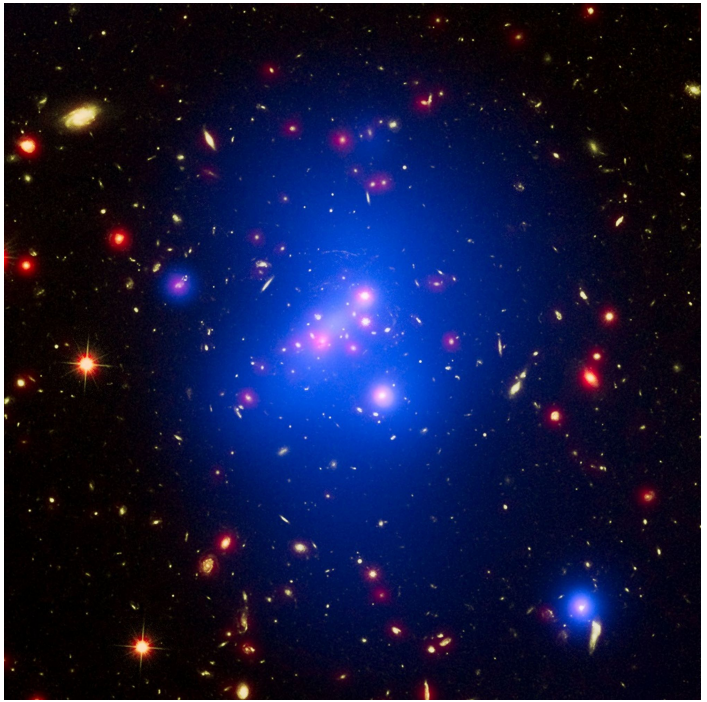
- Title: Constraining Galaxy Cluster Triaxiality via Weak Lensing – I. Preparation for the Rubin Data Beyond Leading Order
- Authors: Srinivasan, Radhakrishnan; Fu, Shenming; Shin, Tae-hyeon; Solomon, Rance; Jones, Deric; Avestruz, Camille; Zhang, Yuanyuan; Aguena, Michel; Combet, Celine; Payerne, Constantin; von der Linden, Anja

Introduction

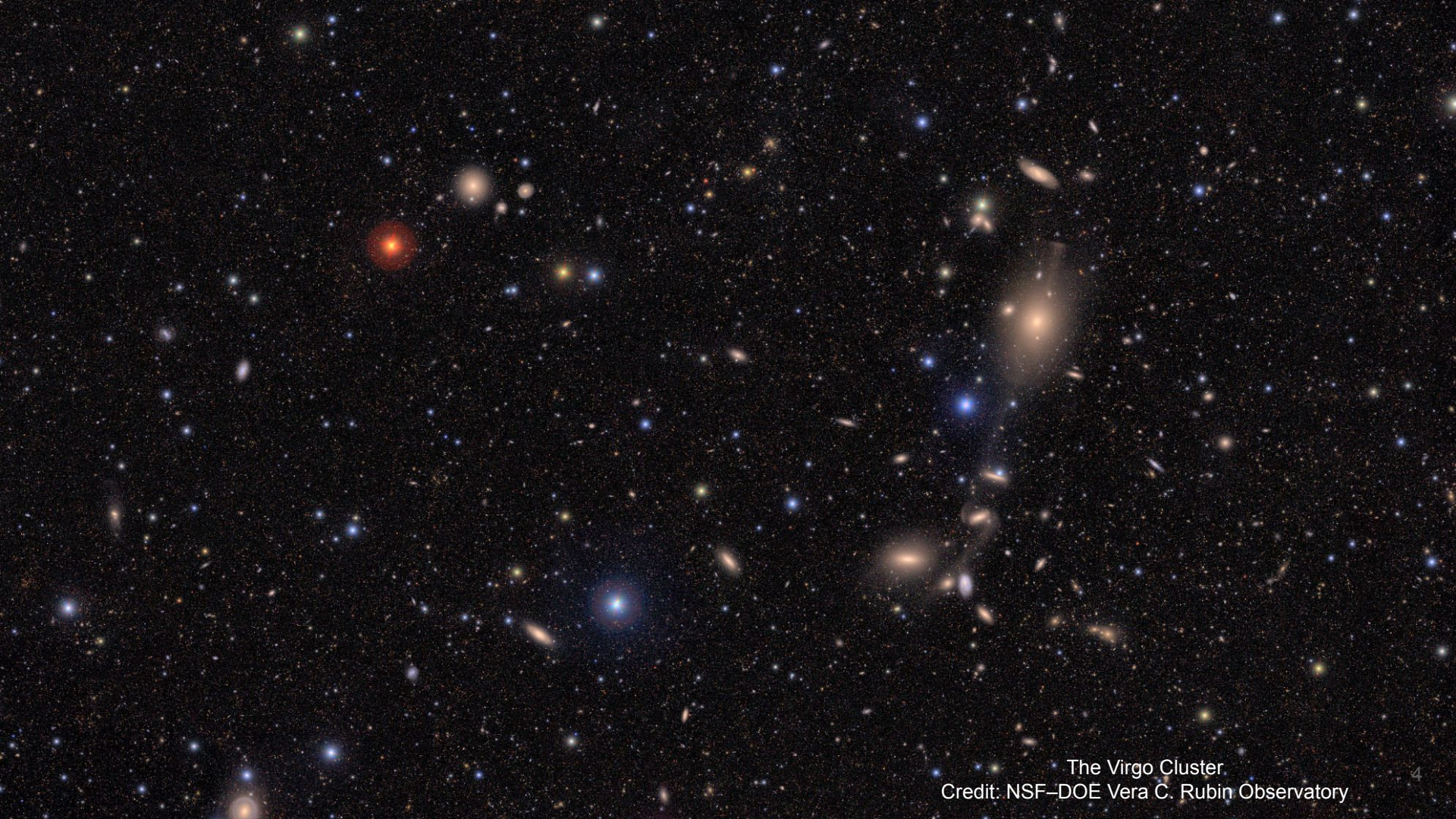
Galaxy clusters: The most Massive structures in the Universe ~ $10^{14}\,M_{\odot}$ - $10^{15}\,M_{\odot}$

- Luminous Red Galaxies (LRGs) (1 %)
- X-ray Emission from Hot Intra-cluster Gas (9 %) also detectable in SZ
- Dark Matter Halo (90 %)

Cosmology: Evolution of the cluster Mass Function



Credit: NASA, ESA, and M. Brodwin (University of Missouri) (IDCS J1426)



The Virgo Cluster
Credit: NSF–DOE Vera C. Rubin Observatory

Introduction

Why study galaxy cluster shapes?

Large scale

- The key to cluster cosmology is **accurate mass measurement**.
- The non-spherical shape of a cluster strongly affects its mass measurement.
- Cluster shapes as a function of redshift can be used to **probe cosmology**.

Small scale

- Cluster shapes can constrain the **self-interaction** of dark matter.
- The distributions of gas, galaxies, and dark matter can inform their coevolution with the environment.
- **Alignment between cluster components and filaments**: from BCG to LSS (from tens of kpc to tens of Mpc).

Introduction

Previous cluster shape measurements

- SDSS redMaPPer clusters with Pcen > 0.9: q ~ 0.57 (Shin+18)
- SDSS LRGs: q ~ 0.61 - 0.78 (Clampitt+16, Robinson+23)
- Hydrosim clusters: q ~ 0.59 (Payerne+23)

Goals of this work

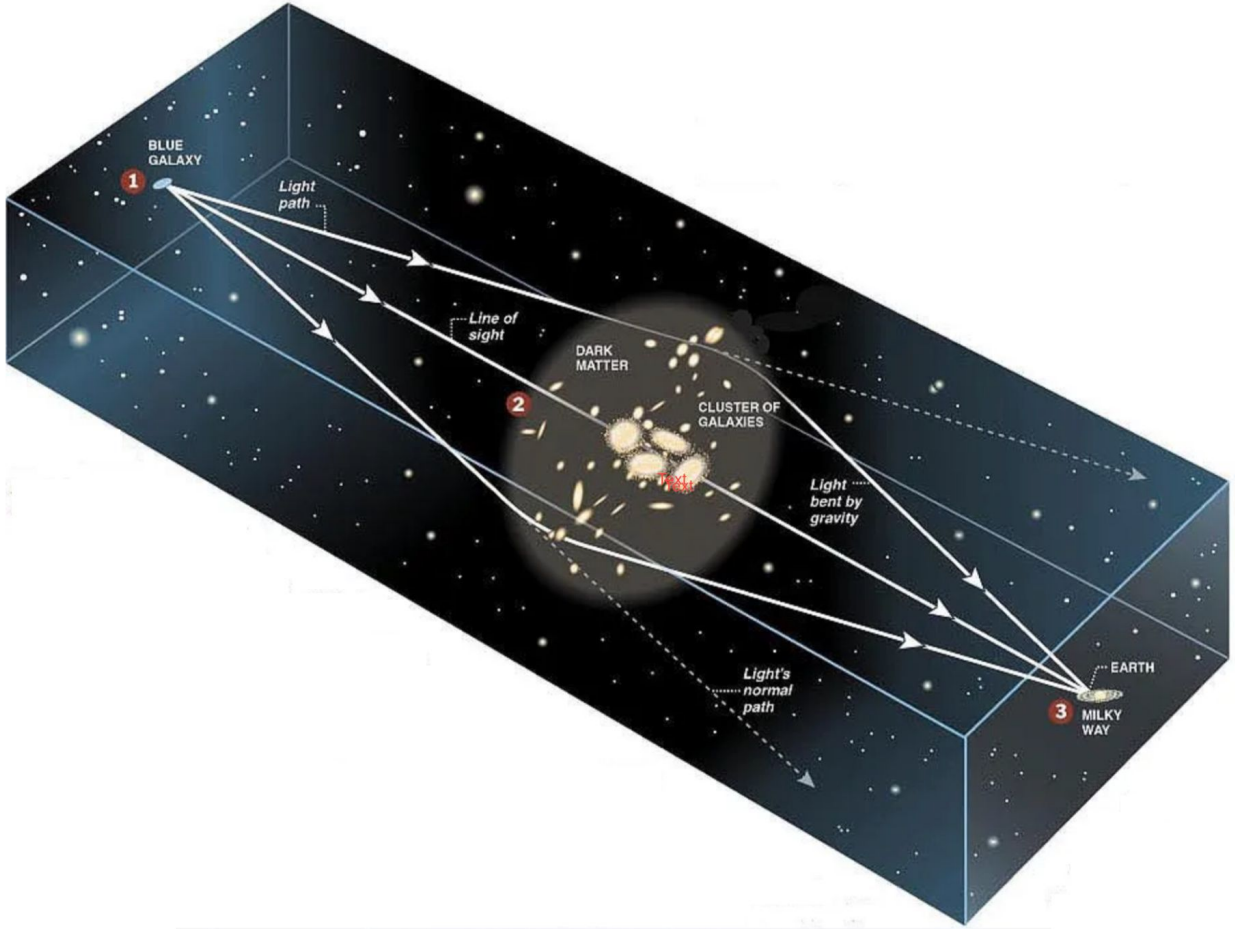
- First measurement of DES-Y3 galaxy cluster shapes via WL.
- Shape as a function cluster properties.
- Initial investigation of systematics.
- Application of CLMM to real data.

Introduction

Gravitational

Weak-Lensing: A powerful measure of the LOS matter distribution (baryonic and dark matter) of the universe.

“Bending” of Light!



Credits: Tony Tyson, Greg Kochanski and ian Dell’Antonio; Frank O’Connell and Jim McManus, adopted from he New York Times

Data

Clusters - DES Y3 redMaPPer with Pcen > 0.9, 0.2 < z < 0.65 for quality ~10k clusters

Shapes - DES Y3 shapes with Metacalibration shear measurement

Photo-zs - DES Y3 DNF (supervised learning)

Simulated mocks - Shear generated by typical elliptical NFW halos for testing cluster shape measurement

Theory & Method

We assume the lens surface density has elliptical contours with fixed ellipticity ϵ.

Multipole expansion for the surface density

$$\Sigma(R,\theta) = \Sigma_0(R) + \Sigma_2(R)\cos 2\theta + \cdots$$

monopole quadrupole

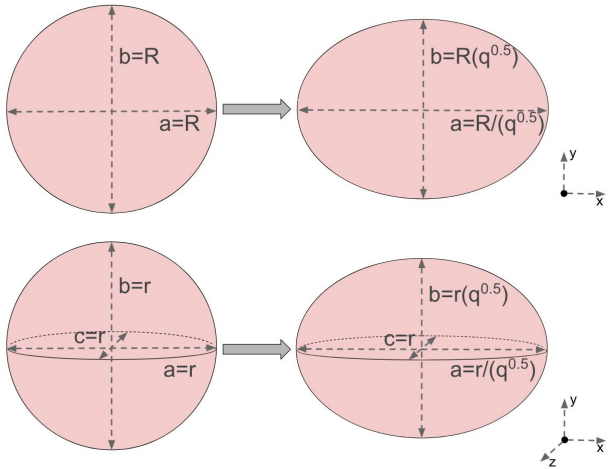
Multipoles (derived from deformation of a spherical profile $\Sigma_{\rm sph}$)

$$\begin{cases} \Sigma_0(R) = \Sigma_{\rm sph}(R)\left[1+\epsilon^2\left(\frac{u}{2}+\frac{u^2}{4}+\frac{1}{4}\frac{{\rm d}u}{{\rm d}\ln R}\right)\right]+\mathcal{O}(\epsilon^3) \\ \Sigma_2(R) = -\epsilon u \Sigma_{\rm sph}(R)+\mathcal{O}(\epsilon^3) \end{cases}$$

New !

$$\epsilon = \frac{1-q}{1+q} \qquad u \equiv \frac{{\rm d}\ln\Sigma_{\rm sph}}{{\rm d}\ln R}$$

$$\Sigma(\sqrt{x^2+y^2}) \rightarrow \Sigma(\sqrt{qx^2+y^2/q})$$



$$\rho(\sqrt{x^2+y^2+z^2}) \rightarrow \rho(\sqrt{qx^2+y^2/q+z^2})$$

- The 2D surface density corresponds to the projection an effective 3D ellipsoid.
- The volume and mass are kept during the deformation.

Theory & Method

How to measure the quadrupole?

Models

$$
\begin{cases}
\Delta\Sigma_{4\theta} = \dfrac{1}{2\pi}\displaystyle\int_0^{2\pi}(\Sigma_{\rm crit}\gamma_1\cos 4\theta + \Sigma_{\rm crit}\gamma_2\sin 4\theta)\mathrm{d}\theta \\
\qquad\qquad = \dfrac{\Sigma_2}{2} - L_1 \quad \text{(only related to matter < R)} \\
\Delta\Sigma_{\rm const} = \dfrac{1}{2\pi}\displaystyle\int_0^{2\pi}\Sigma_{\rm crit}\gamma_1\mathrm{d}\theta = \dfrac{\Sigma_2}{2} - L_2 \quad \text{(only related to matter > R)} \\
L_1(R) = \dfrac{3}{R^4}\displaystyle\int_0^{R} R'^3\Sigma_2(R')\mathrm{d}R' \\
L_2(R) = \displaystyle\int_R^{\infty}\dfrac{\Sigma_2(R')}{R'}\mathrm{d}R' \ .
\end{cases}
$$

Before matching the models and estimators, we apply a few corrections (next slide).

- Source selection: ZMEAN_SOF > z_l + 0.1
- Weight w_i includes the shape weight and $\Sigma_{\rm crit}^{-1}$

Estimators

- Stacking clusters with axes aligned to improve S/N.
- The cluster orientation is determined by satellite (member) distribution.
- *Monopole* generally follows McClintock+19.

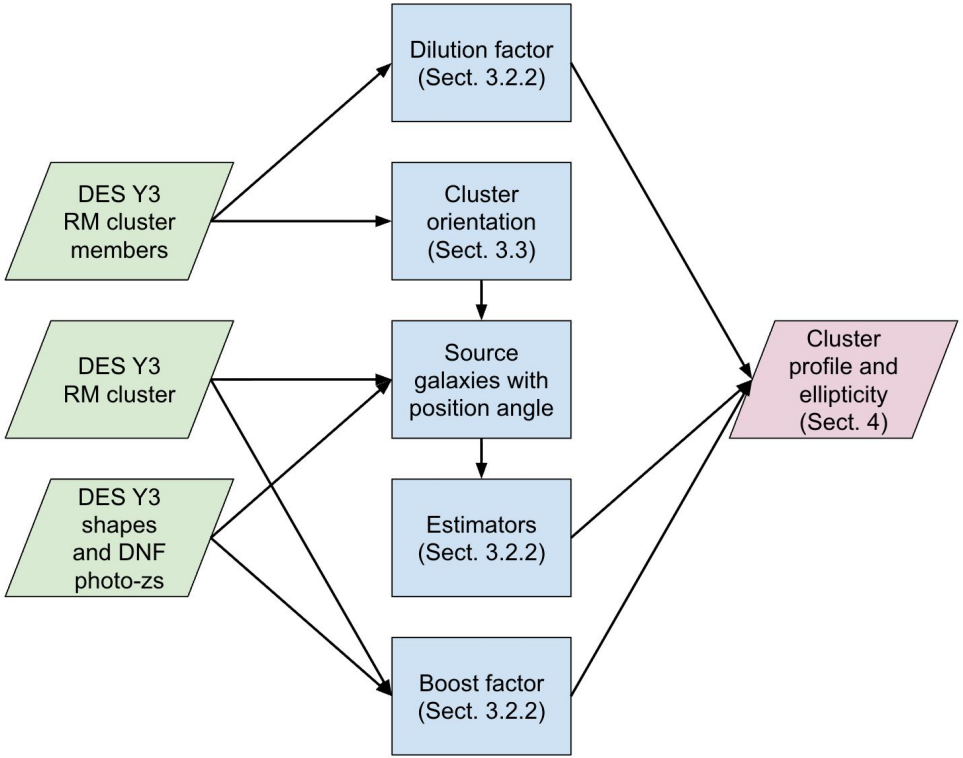
$$\Delta\hat{\Sigma} = \frac{\sum_i w_i e_{{\rm T},i}}{\sum_i w_i {\rm R}_i \Sigma_{{\rm crit},i}^{-1}} = \frac{\langle e_{\rm T}\rangle}{\langle {\rm R}\Sigma_{\rm crit}^{-1}\rangle}$$

Quadrupoles

$$
\begin{cases}
\Delta\hat{\Sigma}_{4\theta} = \dfrac{\sum_i w_i(e_{1,i}\cos 4\theta_i + e_{2,i}\sin 4\theta_i)}{\sum_i w_i {\rm R}_i\Sigma_{{\rm crit},i}^{-1}} \\
\Delta\hat{\Sigma}_{\rm const} = \dfrac{\sum_i w_i e_{1,i}}{\sum_i w_i {\rm R}_i\Sigma_{{\rm crit},i}^{-1}}
\end{cases}
$$

Theory & Method

Analysis pipeline: Data → Processing → Fitting using emcee (MCMC)



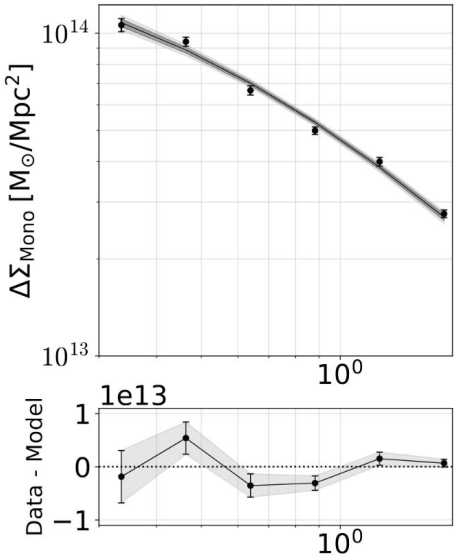
$$\begin{cases} \text{Data} \leftrightarrow \text{Model} \\ \Delta\hat{\Sigma} \leftrightarrow \Delta\Sigma_{\text{final}} = \Delta\Sigma_0/\mathcal{B} \\ \Delta\hat{\Sigma}_{4\theta} \leftrightarrow \Delta\Sigma_{\text{final};\,4\theta} = \Delta\Sigma_{4\theta}(\epsilon_{\text{true}})D(\epsilon_{\text{true}})/\mathcal{B} \\ \Delta\hat{\Sigma}_{\text{const}} \leftrightarrow \Delta\Sigma_{\text{final};\,\text{const}} = \Delta\Sigma_{\text{const}}(\epsilon_{\text{true}})D(\epsilon_{\text{true}})/\mathcal{B} \end{cases}$$

The covariance matrices are computed by bootstrapping.

$$\begin{aligned} &\mathcal{L}(\Delta\Sigma_{\text{final}}, \Delta\Sigma_{\text{final};\,4\theta}, \Delta\Sigma_{\text{final};\,\text{const}}) \\ &= \mathcal{N}(\Delta\Sigma_{\text{final}}|\Delta\hat{\Sigma},\, \sigma_{\Delta\hat{\Sigma}})\mathcal{N}(\Delta\Sigma_{\text{final};\,4\theta}|\Delta\hat{\Sigma}_{4\theta},\, \sigma_{\Delta\hat{\Sigma}_{4\theta}}) \\ &\quad \mathcal{N}(\Delta\Sigma_{\text{final};\,\text{const}}|\Delta\hat{\Sigma}_{\text{const}},\, \sigma_{\Delta\hat{\Sigma}_{\text{const}}}) \end{aligned}$$

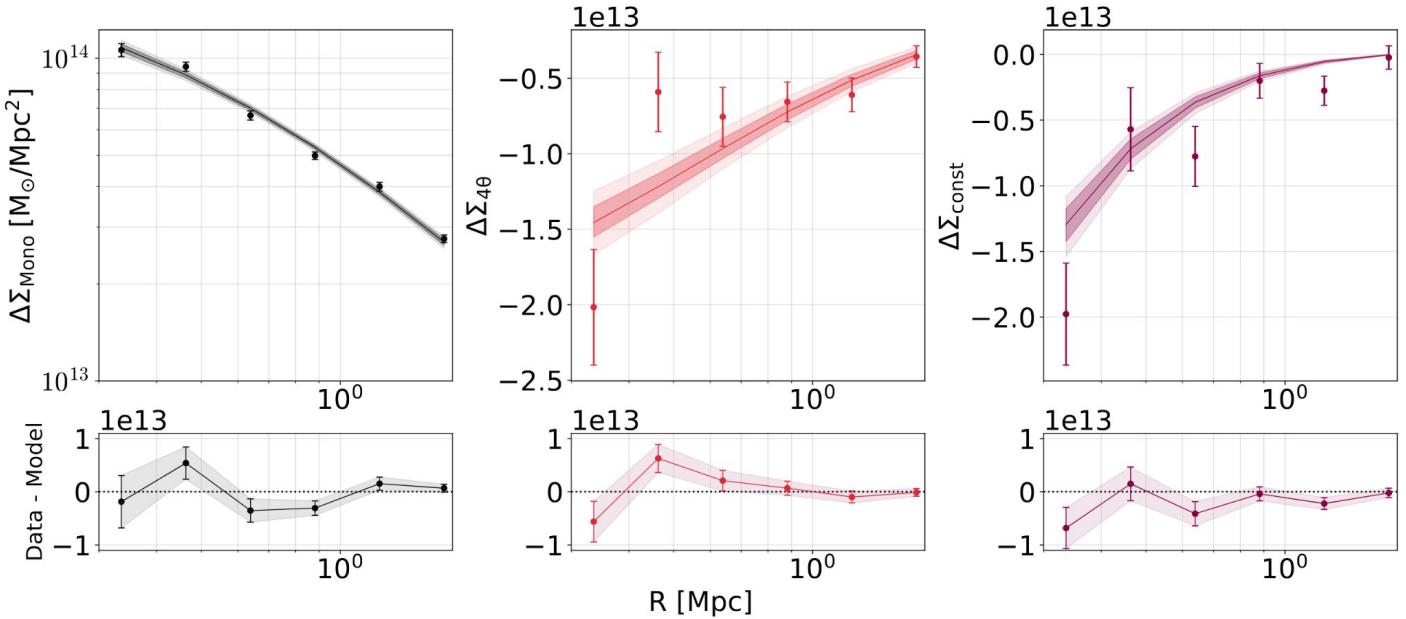
Results

- Ellipticity of the **baseline cluster sample** (DES Y3 redMaPPer and shears, photo-zs)
- $\epsilon = 0.307^{+0.013}_{-0.014}$ ($q = 0.530^{+0.016}_{-0.015}$), $M_{200c} = 1.915^{+0.048}_{-0.051} \cdot 10^{14} M_\odot$, $c_{200c} = 2.74^{+0.16}$



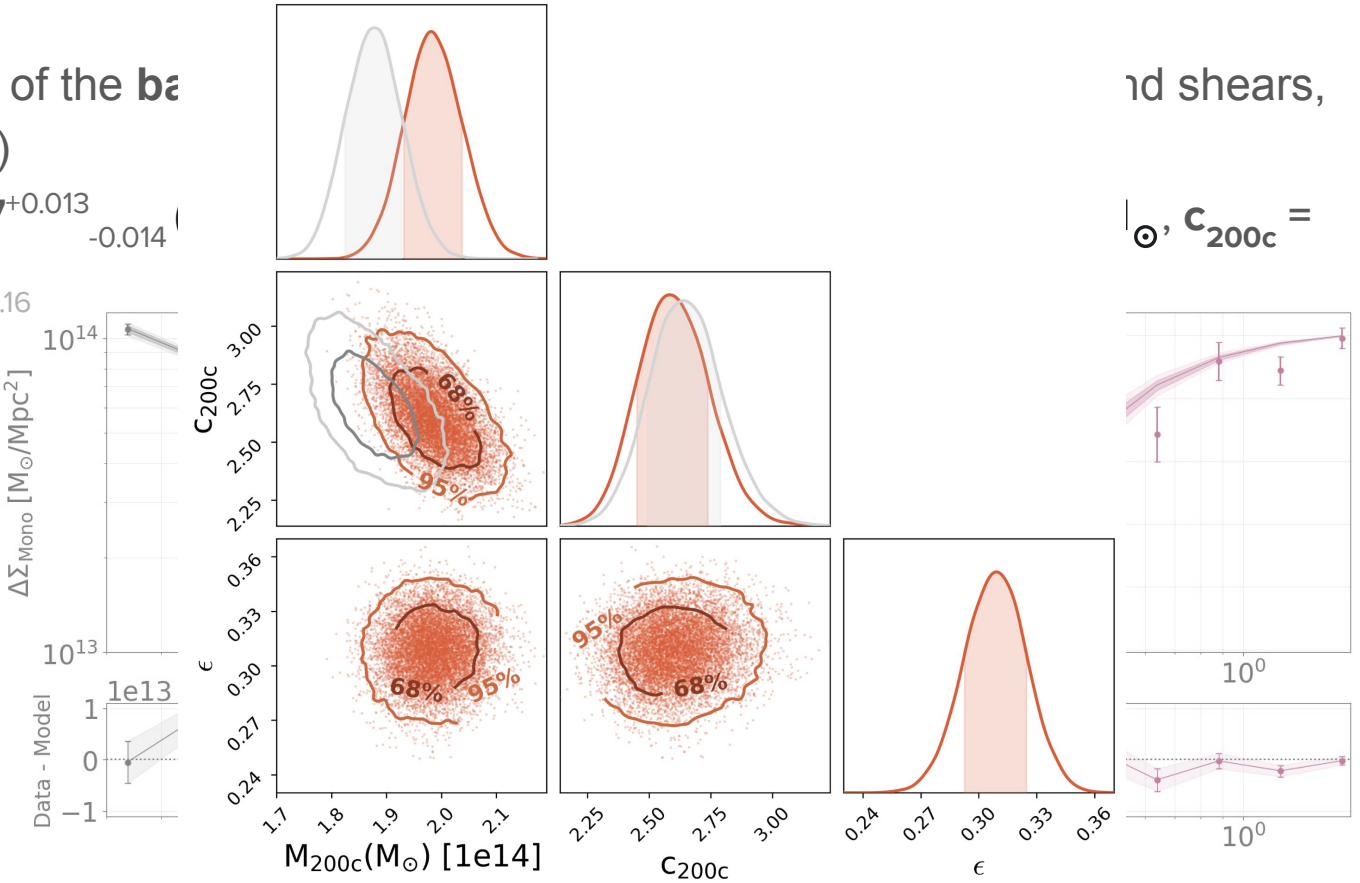
Results

- Ellipticity of the **baseline cluster sample** (DES Y3 redMaPPer and shears, photo-zs)
- $\epsilon = 0.307^{+0.013}_{-0.014}$ ($q = 0.530^{+0.016}_{-0.015}$), $M_{200c} = 1.915^{+0.048}_{-0.051} \cdot 10^{14} M_\odot$, $c_{200c} = 2.74^{+0.16}$



Results

- Ellipticity of the **ba** nd shears, photo-zs)
- $\epsilon = 0.307^{+0.013}_{-0.014}$ ($_{\odot}$, $c_{200c} = 2.74^{+0.16}_{-0.16}$

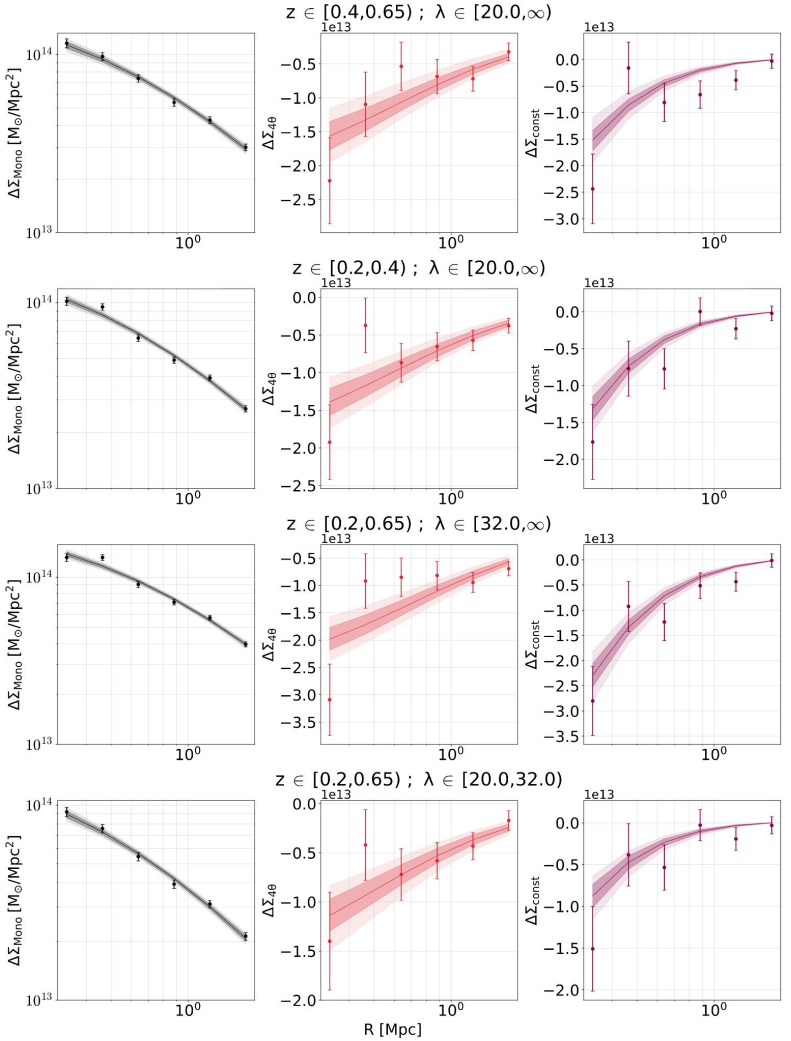


Results

- Split by **richness** or **redshift**
- To test the evolution of ellipticity, split the baseline sample into subsamples (comparable S/N):
  - High z [0.4, 0.65)
  - Low z [0.2, 0.4)

  or

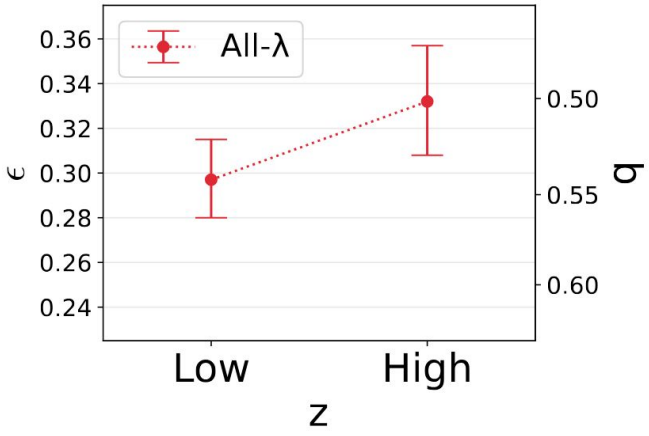
  - High λ [32, ∞)
  - Low λ [0, 32)

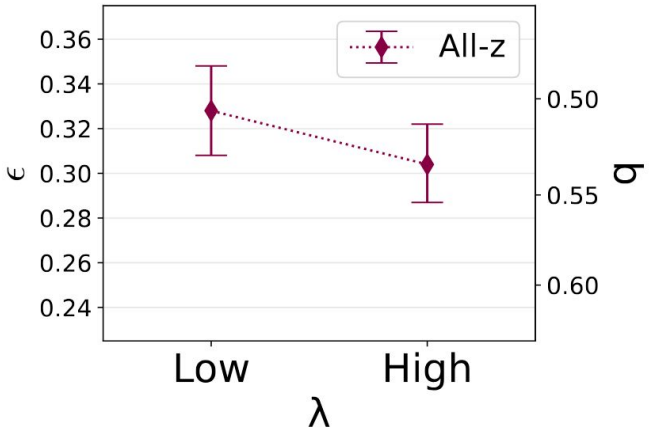


Results

We do not find a statistically significant dependence.

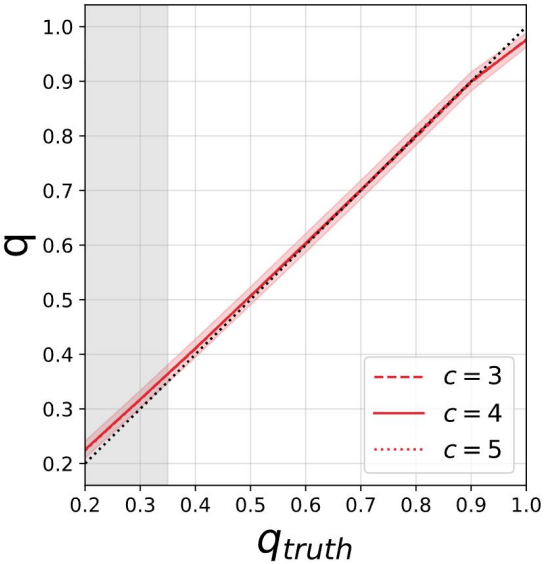
Sample	Ellipticity ϵ	Axis ratio q
Baseline	$0.307^{+0.013}_{-0.014}$	$0.530^{+0.016}_{-0.015}$
High redshift ($z > 0.4$)	$0.332^{+0.025}_{-0.024}$	$0.502^{+0.027}_{-0.029}$
Low redshift ($z < 0.4$)	$0.297^{+0.018}_{-0.017}$	$0.543^{+0.021}_{-0.021}$
High richness ($\lambda > 32$)	$0.304^{+0.018}_{-0.017}$	$0.534^{+0.020}_{-0.021}$
Low richness ($\lambda < 32$)	$0.328^{+0.020}_{-0.020}$	$0.506^{+0.022}_{-0.023}$

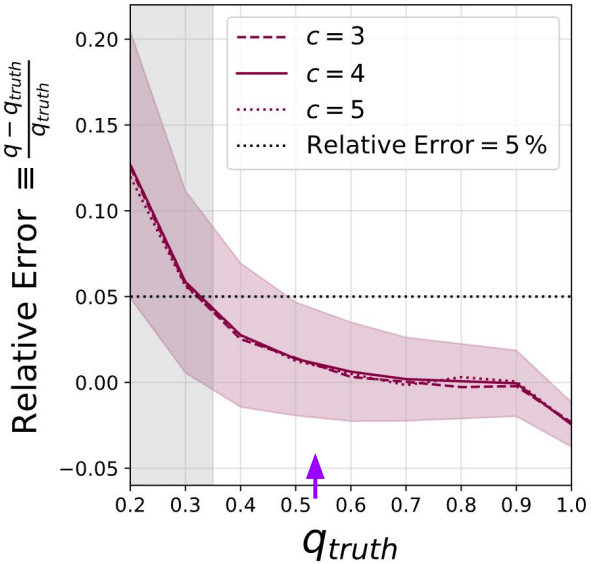




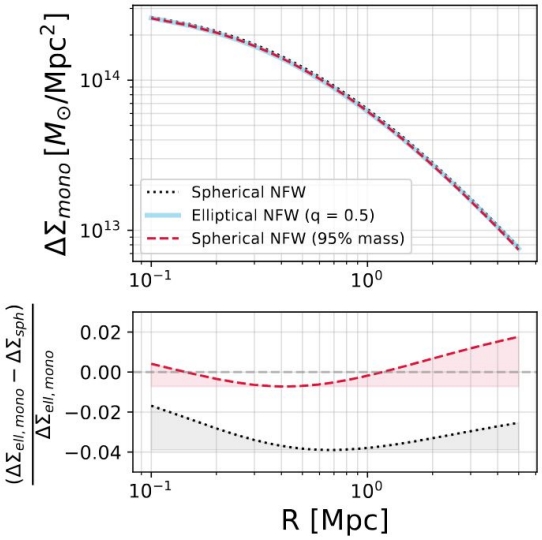
Discussion

Halo ellipticity measurement bias (due to Taylor expansion of the ellipticity; tested by mock catalogs)



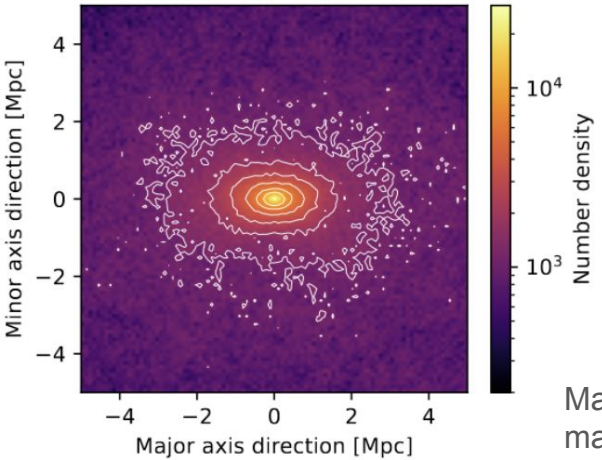


Mass measurement bias (Spherical ΔΣ vs Monopole ΔΣ: difference due to the ϵ^2 term)

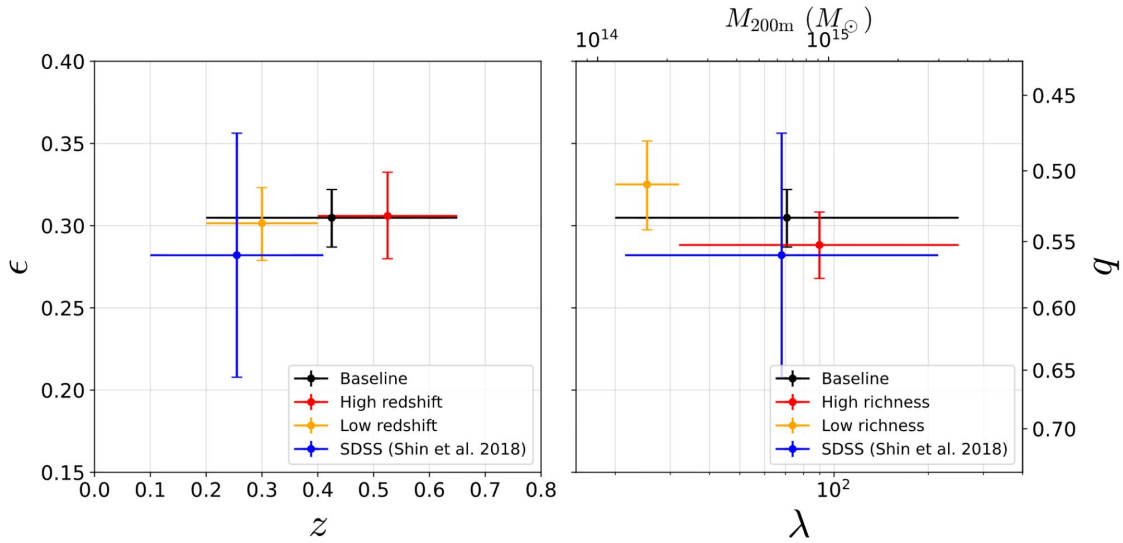


Discussion

- Comparison with previous work – consistent with SDSS clusters (Shin+18)
- Galaxy density profile: nearly fixed axis ratio when R < 2 Mpc



MagLim galaxy number density stacked along cluster major axes.



Comparison of projected halo ellipticity measurements.

Conclusion

We study the triaxiality of **DES Y3** redMaPPer clusters through WL multipole expansion up to the second order in ellipticity.

- We chose high centering probability clusters (Pcen > 0.9), with $0.2 < z < 0.65$
- We obtain an effective ellipticity of $\boldsymbol{\epsilon = 0.306^{+0.017}_{-0.019}}$ (axis ratio $\mathbf{q = 0.531^{+0.021}_{-0.020}}$).
- We correct for boost factor (contamination from cluster galaxies) and dilution factor (angle misalignment of haloes during stacking)
- Dividing the sample into redshift and richness bins shows no statistical evidence for evolution of ϵ. Data from HSC, LSST, Euclid, Roman, etc. will improve this measurement.

Paper II, III, ... and onwards

Paper II will focus on

- **Cosmological simulations** (e.g. SkySim5000) to improve our understanding of systematics.
  - Comparing the orientations/ellipticities of the cluster halo and neighboring filaments; 2-halo modelling.
  - Improving dilution factor predictions from simple MC simulations.
  - Evolution of ellipticity with cluster properties like mass, redshift, dynamical state, etc.
  - Studying the impact of selection effects due to projection.
  - Testing the offset between the particle mass center and the central galaxy (miscentering).
  - Using Simulation-Based Inference for implicit likelihood computation

Paper III will focus on **observational data** especially the LSST Data Preview 2 (DP2) or Data Release 1 (DR1) once they are available. Also we will attempt direct eNFW fitting and test the effect of miscentering (comparison between CG and X-ray/SZ/mass-map centers).

Appendix

Theory & Method

Contamination of cluster galaxies & Boost factor

Due to the photo-z error, some (unlensed) cluster galaxies can be recognized as background galaxies and thus dilute the lensing signal.

To correct for it, we use the photo-z to estimate the boost factor in each radial bin (Varga+19).

$$P(z|R) = f_{\rm cl}(R)P_{\rm m}(z) + (1 - f_{\rm cl}(R))P_{\rm bg}(z)$$

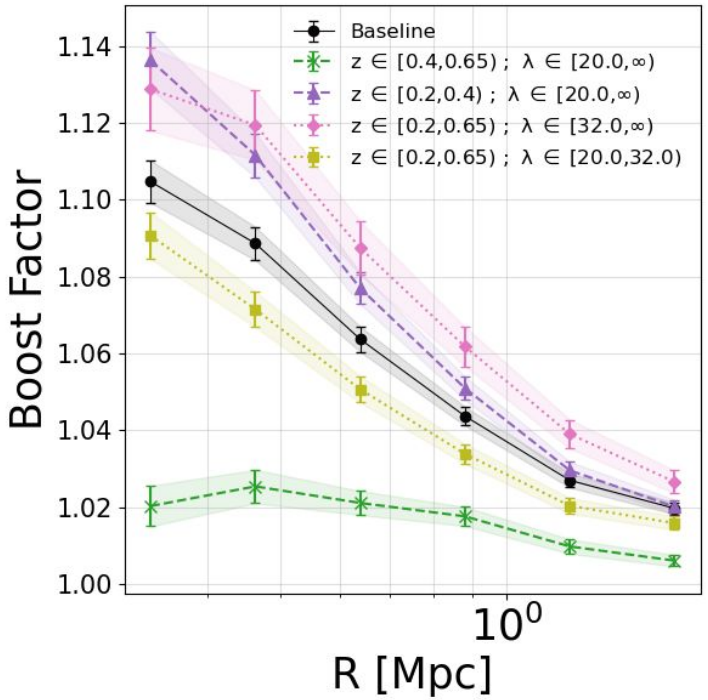
observed photo-z distribution

fraction of cluster galaxies

redshift distribution of cluster galaxies (Gaussian)

redshift distribution of background galaxies (estimated by galaxies far away from the cluster)

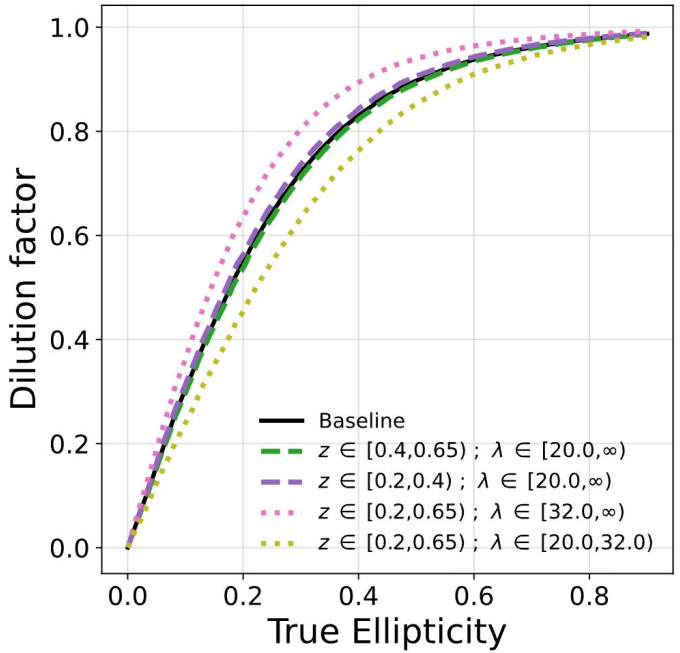
$$\mathcal{B}(R) = \frac{1}{1 - f_{\rm cl}(R)}$$



Theory & Method

Misalignment angle & Dilution correction

- The satellite distribution orientation may not trace the halo well.
  - Misalignment angle θ_0 between their major axes
  - This dilutes the quadrupole signal (the cluster looks “rounder”) by $\cos 2\theta_0$.
- We use Monte Carlo to compute the dilution factor and address these biases.
  - Poisson bias (limited number of satellites)
  - Edge bias (R_λ cut)
  - Interloper bias (line of sight non-satellites)
  - Similar to Shin+18 with finer modeling
- Cosmological simulations can further improve this analysis (next slide).



Results

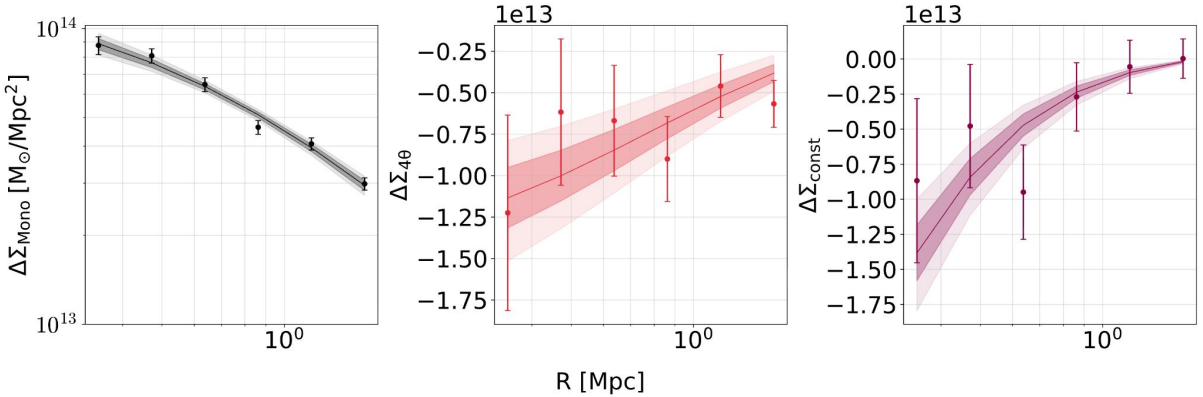
Validation tests

- Comparing to Y1 redMaPPer clusters (with dilution factor & without boost factor)

  $\epsilon = 0.309^{+0.027}_{-0.027}$

  $q = 0.529^{+0.031}_{-0.031}$

- Splitting the Y1 clusters according to McClintock+19 into 4 richness and 3 redshift bins
- Mass bias = $(M - M_{M19})/M_{M19}$ about 10%

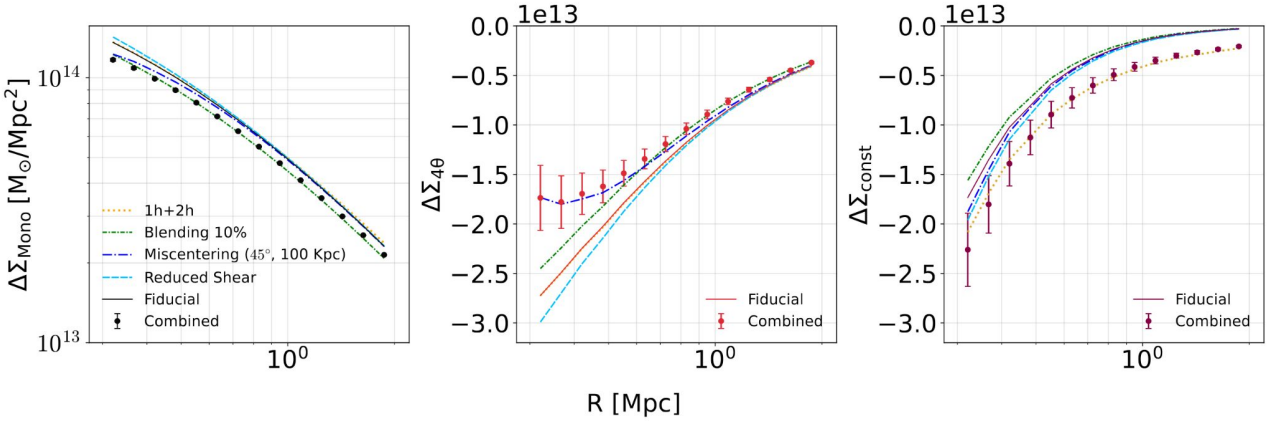


Mass difference (%)	$z \in [0.2, 0.35)$	$z \in [0.35, 0.5)$	$z \in [0.5, 0.65)$
$\lambda \in [20, 30)$	-0.5 ± 11.2	-5.1 ± 8.4	17.8 ± 10.2
$\lambda \in [30, 45)$	-7.5 ± 7.2	-8.4 ± 8.3	-12.8 ± 11.9
$\lambda \in [45, 60)$	-5.1 ± 9.9	-3.3 ± 9.7	-15.2 ± 14.5
$\lambda \in [60, \infty)$	-1.9 ± 9.9	-8.8 ± 8.9	-6.4 ± 14.7

Discussion

Systematics:

- Blending
- Convergence
- Miscentering
- 2-halo



Key takeaway: Stacked Ellipticity measurement is robust.

Systematics	ϵ	$\epsilon/\epsilon_{\rm truth}-1$	q	$q/q_{\rm truth}-1$
Fiducial	0.328 ± 0.004	-0.016 ± 0.012	0.506 ± 0.005	0.012 ± 0.010
Blending 1 %	0.328 ± 0.004	-0.016 ± 0.012	0.506 ± 0.005	0.012 ± 0.010
Blending 10 %	0.329 ± 0.004	-0.013 ± 0.012	0.505 ± 0.005	0.010 ± 0.010
Reduced shear	0.335 ± 0.004	0.005 ± 0.012	0.498 ± 0.004	-0.004 ± 0.008
Miscentering $(0°, 100\,\mathrm{kpc})$	0.345 ± 0.004	0.035 ± 0.012	0.487 ± 0.004	-0.026 ± 0.008
Miscentering $(45°, 100\,\mathrm{kpc})$	0.315 ± 0.004	-0.055 ± 0.012	0.521 ± 0.005	0.042 ± 0.010
Miscentering $(90°, 100\,\mathrm{kpc})$	0.283 ± 0.004	-0.151 ± 0.012	0.559 ± 0.005	0.118 ± 0.010
2-halo	0.331 ± 0.004	-0.007 ± 0.012	0.503 ± 0.005	0.006 ± 0.010
*Combined	0.324 ± 0.004	-0.028 ± 0.012	0.511 ± 0.005	0.022 ± 0.010